Available online at www.sciencedirect.com
SCIENCE DIRECT
Carbohydrate Research 341 (2006) 1398–1407
Carbohydrate RESEARCH

Synthesis, nucleic acid hybridization properties and molecular modelling studies of conformationally restricted 3′-*O*,4′-*C*-methylene-linked α-L-ribonucleotides

Andreas S. Madsen, Patrick J. Hrdlicka, T. Santhosh Kumar and Jesper Wengel*

Nucleic Acid Center,† Department of Chemistry, University of Southern Denmark, DK-5230 Odense M, Denmark

Received 14 March 2006; received in revised form 7 April 2006; accepted 8 April 2006
Available online 18 May 2006

Abstract—Nucleotides with conformationally restricted carbohydrate rings such as locked nucleic acid (LNA), α-L-LNA or 2′,5′-linked 3′-*O*,4′-*C*-methyleribonucleotides exhibit significant potential as building blocks for antigene and antisense strategies. 2′,5′-Linked α-L-*ribo* configured monomer **X** (termed α-L-ONA) was designed as a potential structural mimic of α-L-LNA. The corresponding phosphoramidite building block of monomer **X** was obtained in five steps (10% overall yield) from the easily obtainable thymine derivative **1**. Incorporation of monomer **X** into oligodeoxyribonucleotides (ONs) results in dramatically decreased thermal stabilities with DNA/RNA complements (ΔT_m/mod = −11.5 to −17.0 °C) compared to unmodified reference ONs. Less pronounced decreases (ΔT_m/mod = −4.5 to −8.5 °C) are observed when monomer **X** is incorporated into triplex forming ONs and targeted against double-stranded DNA (parallel orientation, pyrimidine motif). This biophysical data, together with modelling studies, suggest that 2′,5′-linked α-L-ONA is a poor structural mimic of α-L-LNA.
© 2006 Elsevier Ltd. All rights reserved.

Keywords: LNA; 2′,5′-Linked nucleic acids; Conformationally restricted nucleosides; Oligonucleotides; Oxetane

1. Introduction

The antigene and antisense strategies, that is, targeting of double-stranded DNA and single-stranded RNA with exogenous probes, respectively, continue to be highly desirable approaches to achieve specific control of gene expression.[1] During the past two decades, substantial efforts have been directed towards developing modified oligonucleotide probes with improved antigene or antisense characteristics such as increased target affinity and mismatch discrimination and enhanced stability towards enzymatic degradation.[2,3] A particularly successful approach to realize this has been to modify oligodeoxyribonucleotides (ONs) with nucleotides that have conformationally restricted carbohydrate rings.[4–7]

The flexible furanose ring of unmodified nucleosides adopts many different conformations in solution, although they tend to cluster in two regions that are classified as belonging to either the North (*N*) or South (*S*) part of the pseudorotational cycle.[8] The dioxabicyclo-[2.2.1]heptane skeletons of LNA (locked nucleic acid, β-D-*ribo* configuration, Fig. 1)[9–13] and its diastereomer α-L-LNA (α-L-*ribo* configuration, Fig. 1)[14–16] efficiently lock the furanose ring in an *N*-type conformation. (The furanose ring of α-L-LNA is, according to definitions, conformationally restricted in an *N*-type conformation as a result of the L-configuration; however, α-L-LNA does not overlay onto a typical *N*-type framework but rather overlays an *S*-type framework.) A single incorporation of an LNA or α-L-LNA building block into ONs induces, depending on sequence length and composition, large increases in thermal stability towards complementary DNA or RNA of up to +10 °C relative to unmodified ONs.[9–16] NMR studies have suggested that the increases in thermal stability are related to the

† A research center funded by the Danish National Research Foundation for studies on nucleic acid chemical biology.

* Corresponding author. Tel.: +45 6550 2510; fax: +45 6615 8780; e-mail: jwe@chem.sdu.dk

0008-6215/$ - see front matter © 2006 Elsevier Ltd. All rights reserved.
doi:10.1016/j.carres.2006.04.010

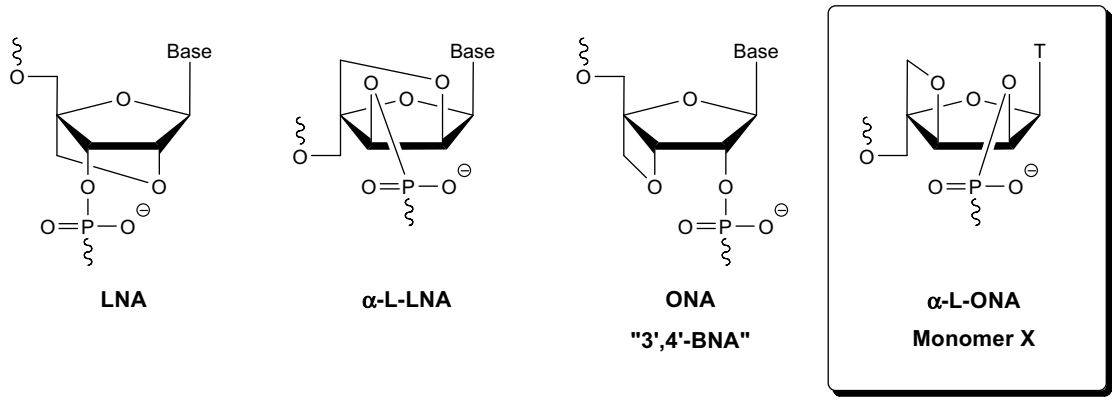

Figure 1. Structures of LNA,[9–13] α-L-LNA[14–16] and ONA (previously termed 3′,4′-BNA)[38–40] along with the novel α-L-ONA (3′-*O*,4′-*C*-methylene-linked α-L-ribonucleotide, monomer **X**) reported herein. T = Thymin-1-yl.

predisposition of LNA to behave as an A-type (RNA) mimic with regard to helical structure[17,18] whereas α-L-LNA behaves as an B-type (DNA) mimic.[19,20] The potential of LNA and α-L-LNA as triplex forming oligonucleotides (TFOs) is obvious, as a single incorporation of LNA[21–24] or α-L-LNA[25] nucleotides into triplex forming ONs generally induces very prominent increases in thermal stability of up to +10.0 and +6.0 °C, respectively.

2′,5′-Linked nucleic acids (2′,5′-NAs)[26–28] have been suggested as potential antisense and antigene probes due to the following properties: (a) 2′,5′-NAs form duplexes with normal RNA (i.e., 3′,5′-linked RNA) albeit they bind with lower affinity than isosequential DNA, (b) 2′,5′-NAs display a remarkable preference for complexation with RNA complements, (c) homopyrimidine chimeras of 2′,5′-linked DNA and normal DNA exhibit significantly increased thermal affinity towards double-stranded DNA compared to an unmodified ON and (d) 2′,5′-NAs exhibit high resistance to nuclease digestion.[29–35]

2′,5′- and 3′,5′-NAs have been suggested to exhibit an interesting inverse relationship between nucleotide geometry and phosphodiester linkage (Fig. 2), that is, *S*-type 2′,5′-NAs adopt a compact backbone (intrastrand distance between two phosphorous atoms is below 6 Å) similar to that of *N*-type 3′,5′-NAs, whereas *N*-type 2′,5′-NAs adopt an extended backbone (P–P distance above 7 Å) similar to that of *S*-type 3′,5′-NAs.[36,37] The preference for complexation with RNA complements and prominent stabilization of triplexes with 2′,5′-NAs has therefore, and in the light of the properties of *N*-type nucleosides such as LNA, been suggested to arise from a tendency of 2′,5′-NAs to adopt compact *S*-type furanose conformations.[35]

	β-D-*ribo*	
	N-type	*S*-type
3′,5′-linked	Compact	Extended
2′,5′-linked	Extended	Compact

Figure 2. Nucleotide conformation of β-D-*ribo* configured nucleotides having *N*- and *S*-type sugar puckering, emphasizing the inverse relationship between intrastrand P–P distance (compact vs extended) and the phosphodiester linkage (3′,5′ vs 2′,5′).

The synthesis of bicyclic 2′,5′-linked nucleosides in which the furanose ring is conformationally biased towards a compact *S*-type conformation, has recently been reported.[38–41] Incorporation of 3′-*O*,4′-*C*-methyleribonucleotides (Fig. 1, herein termed ONA for 'oxetane nucleic acid') into ONs results in significantly decreased thermal affinities towards DNA complements while the affinity towards RNA complements is virtually unchanged compared to unmodified ONs.[38] The potential of ONA as TFOs has been evaluated in a single study but, arguably due to suboptimal sequence design, ONA was found to destabilize triplexes,[40] and a more thorough evaluation of ONA as TFOs is therefore awaited.

The inverse relationship of nucleotide geometry and phosphodiester linkage between 2′,5′- and 3′,5′-NAs (Fig. 2) suggests that the 2′,5′-linked ONA mimics the structure of LNA and that a 2′,5′-linked bicyclic nucleoside with α-L-*ribo* configuration such as monomer **X** (Fig. 1) would behave as a structural mimic of α-L-LNA, which is known to adopt an extended backbone.[19,20] The incorporation of a 2′,5′-linked nucleoside with inverted stereochemistry at the C2′-, C3′- and C4′-positions (relative to normal RNA) into ONs has not been reported and we therefore set out to synthesize monomer **X** and to evaluate this missing member of the bicyclic nucleoside family.

2. Results and discussion

Phosphoramidite **6** was identified as a suitable building block for incorporation of monomer **X** using automated DNA synthesis. Retrosynthetic analysis revealed bicyclic

nucleoside **4** as a key intermediate, which was expected to be obtainable from known thymine derivative **1**[42] after appropriate blocking of the C2′-hydroxy group with a base stable protecting group to avoid competing α-L-LNA nucleoside formation during ring closure (Scheme 1). Tetrahydropyranylation of alcohol **1** was therefore attempted using 3,4-dihydro-2*H*-pyran (DHP) in anhydrous dioxane and pyridinium *p*-toluenesulfonate (PPTS) as catalyst. However, the desired O2′-THP protected nucleoside was only obtained in an unsatisfactory yield of 20% (data not shown), which did not improve by changing the solvent and/or catalyst.[43,44] Protection of the C2′-hydroxy group proved to be notoriously difficult as introduction of the well-established MOM or TBDMS groups or the recently described dimethylthiocarbamate group[45] also were unsuccessful, most likely as a consequence of the steric hindrance exerted on the C2′-position by the 1,3-cis relationship of the thymine and C3′-benzyloxy moieties.

These difficulties prompted us to investigate an alternative route to phosphoramidite **6**, which is based on selective ring closure (Scheme 1). Debenzylation of alcohol **1** by catalytic hydrogenation using $Pd(OH)_2/C$ as catalyst afforded diol **2** in satisfying 92% yield. Ring closure to give bicyclic nucleosides has typically been carried out via intramolecular nucleophilic substitution under alkaline conditions.[9,10,46,47] Because both hydroxyl groups of nucleoside **2** may act as nucleophiles, two products must be expected, that is, the desired α-L-ONA nucleoside and the corresponding α-L-LNA nucleoside. Previous examples of ring closure in related β-D-*ribo* configured compounds with two potentially nucleophilic hydroxy groups include a bicyclic derivative of 3′-*C*-ethynyluridine[47] and 3′-*O*,4′-*C*-methyleneribonucleotides,[46] which afforded the desired oxetane derivatives in good yields.

Among the various conditions attempted, including LiHMDS in THF,[46] NaH in THF[9,10] or saturated methanolic ammonia,[47] the most satisfactory was treatment of nucleoside **2** with dilute aqueous sodium hydroxide. The method afforded an inseparable mixture (~3:2 by ^{1}H NMR) of two compounds, tentatively assigned as (1*S*,3*R*,4*S*,5*R*)-4-hydroxy-1-methanesulfonyloxymethyl-3-(thymin-1-yl)-2,6-dioxabicyclo[3.2.0]heptane and (1*S*,3*R*,4*S*,7*R*)-7-hydroxy-1-methanesulfonyloxymethyl-3-(thymin-1-yl)-2,5-dioxabicyclo[2.2.1]heptane, that is, the α-L-ONA and α-L-LNA intermediates, respectively. The mixture was subsequently subjected to sodium benzoate in DMF from which α-L-ONA nucleoside **3** was isolated in 25% yield (over two steps from **2**). Subsequent O5′-deacylation of bicyclic nucleoside **3** with saturated methanolic ammonia furnished diol **4** in 84% yield. The primary C5′-hydroxy group of diol **4** was protected as a 4,4′-dimethoxytrityl (DMTr) ether using

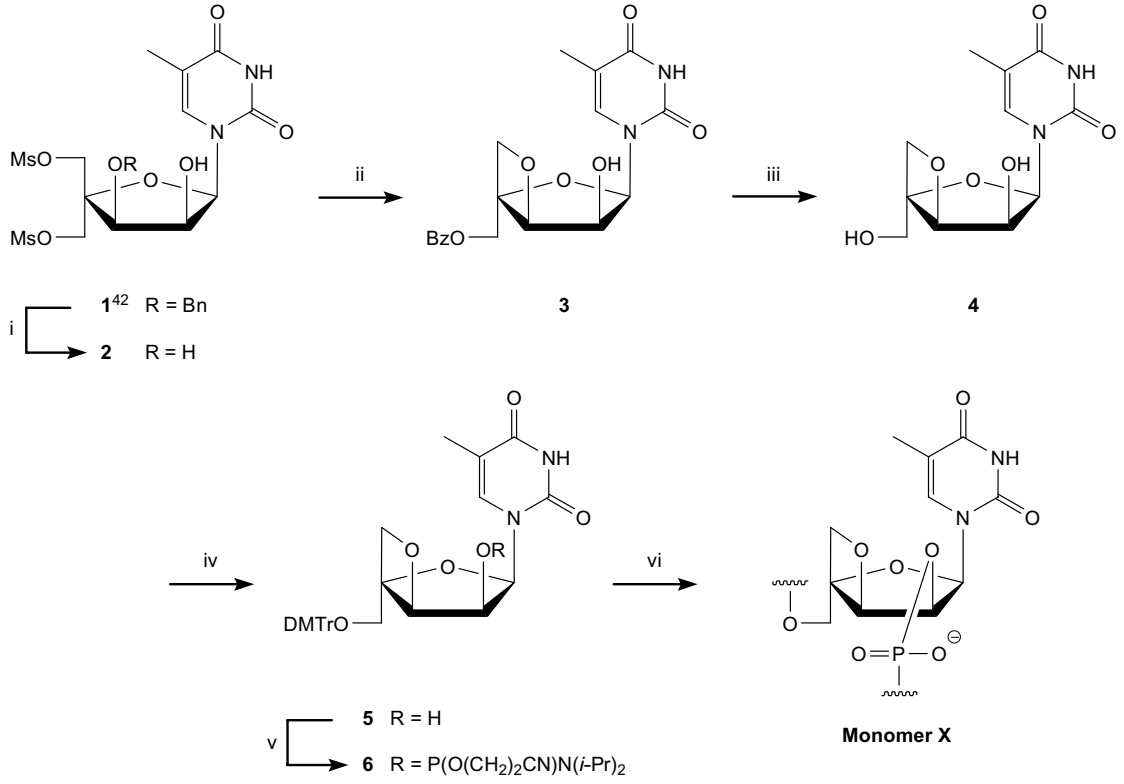

Scheme 1. Reagents, conditions and yields: (i) H_2/(20% $Pd(OH)_2/C$), EtOAc, rt (92%); (ii) (a) aq NaOH, 0–4 °C, (b) NaOBz, DMF, 60–75 °C (25% over two steps); (iii) satd NH_3/CH_3OH, rt (84%); (iv) DMTrCl, pyridine, rt (85%); (v) $NC(CH_2)_2OP(Cl)N(i\text{-}Pr)_2$, $EtN(i\text{-}Pr)_2$, CH_2Cl_2, rt (58%); (vi) DNA synthesizer.

standard conditions to furnish nucleoside **5** in 85% yield. Taking the difficulties associated with O2′-protection of nucleoside **1** into account, nucleoside **5** underwent standard phosphitylation to give phosphoramidite **6** in 58% yield surprisingly easily.

2.1. Structural verification of bicyclic nucleoside 4

The following NMR observations ascertained the proposed 2,6-dioxabicyclo[3.2.0]heptane skeleton of nucleoside **4** and ruled out a 2,5-dioxabicyclo[2.2.1]heptane skeleton corresponding to an α-L-LNA nucleoside: (a) in the ^{1}H NMR spectrum H2′ couples to H1′, 2′-OH and H3′ with coupling constants J >5 Hz, while these coupling constants are very small for α-L-LNA nucleosides (J <2 Hz),[16] (b) the signal from 2′-OH is observed as an exchangeable doublet at ~5.8 ppm, (c) no signal corresponding to a 3′-OH group is observed and (d) the oxetane ring protons H5″ appear as two doublets (AB-system) at 4.12 and 4.69 ppm. Furthermore NOE difference spectroscopy identified key contacts between H1′/H2′ (14%) and H2′/H3′ (11%), indicating a cis relationship between these protons (Fig. 3; NOE-enhancements are given as an average of the two values observed upon individual irradiation of the protons in question). In addition, the observed NOE contact between H6/H5″$_A$ (7%) (H5″$_A$ is tentatively assigned as the H5″ proton closest to H6), indicates a cis relationship between the nucleobase and the oxymethylene bridge.

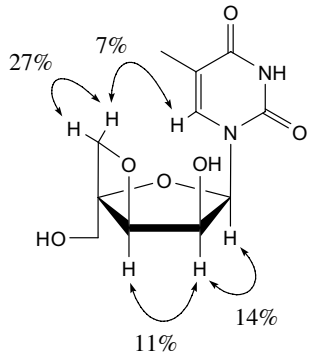

Figure 3. Key NOE contacts in bicyclic nucleoside **4**. (NOE-enhancements are an average of the two values observed upon individual irradiation of the protons in question.)

2.2. Synthesis of ONs

Incorporation of phosphoramidite **6** into oligodeoxyribonucleotides (ONs) was performed on a 0.2 μmol scale using an automated DNA synthesizer. Standard procedures were used resulting in stepwise coupling yields >98% of phosphoramidite **6** (20 min coupling time) and >99% of unmodified deoxyribonucleotide phosphoramidites (2 min coupling time). The composition and purity of the resulting α-L-ONAs **ON3**–**ON5**, **ON7**–**ON8**, **ON10**–**ON11** and **ON13**–**ON14** (Tables 1 and 2) were verified by MALDI-MS (Table S1) and ion-exchange HPLC, respectively.

2.3. Duplex thermal denaturation studies

The effect on duplex stability upon incorporation of monomer **X** into ONs was evaluated by UV-thermal duplex denaturation studies using medium or high salt buffer conditions ([Na^+] = 110 and 710 mM, respectively, pH 7.0, Table 1). Unless otherwise noted, the UV-thermal denaturation curves displayed smooth sigmoidal

Table 1. Thermal denaturation studies of duplexes at different salt concentrations[a]

		T_m (ΔT_m/mod)/°C			
		Medium salt		High salt	
		DNA	RNA	DNA	RNA
ON1	5′-GTG ATA TGC	30.0[b]	27.5	36.0[b]	34.0
ON2	5′-GCA TAT CAC	30.0[b]	27.0	36.0[b]	34.5
ON3	5′-GTG AXA TGC	14.0 (−16.0)	14.5 (−13.0)	21.5[c] (−14.5)	22.0[d] (−12.0)
ON4	5′-GCA **X**A**X** CAC	<10	<10	<10	12.0 (−11.5)
ON5	5′-G**X**G AXA **X**GC	<10	<10	<10	<10
ON6	5′-GCG TTT TTT GCT	46.5	42.5	nd	nd
ON7	5′-GCG TTT TT**X** GCT	29.5 (−17.0)	31.0 (−11.5)	nd	nd
ON8	5′-GCG TTT T**X**X GCT	16.5 (−15.0)	22.5 (−10.0)	nd	nd

[a] Thermal denaturation temperatures (T_m-values) of **ON1**–**ON8** towards DNA/RNA complements [T_m values/°C (ΔT_m/mod = change in T_m value per incorporation of monomer **X** relative to DNA:DNA or DNA:RNA reference duplex)] measured as the maximum of the first derivative of the melting curve (A_{260} vs temperature) recorded in medium salt buffer (100 mM NaCl, 0.1 mM EDTA, adjusted to pH 7.0 by 10 mM NaH_2PO_4/5 mM Na_2HPO_4) or high salt buffer (as for medium salt buffer except 700 mM NaCl) using 1.0 μM concentrations of the two complementary strands and a temperature ramp of 1.0 °C/min. T_m values are averages of at least two measurements; A = adenine-9-yl DNA monomer, C = cytosine-1-yl DNA monomer, G = guanine-9-yl DNA monomer, T = thymin-1-yl DNA monomer, see Scheme 1 for the structure of monomer **X**. nd = not determined.

[b] **ON1** and **ON2** are complementary.

[c] T_m values (°C) towards DNA strands containing a single mismatch in the central position C/G/T: <10/21.0/<10.

[d] T_m values (°C) towards RNA strands containing a single mismatch in the central position C/G/U: <10/24.5/<10.

Table 2. Thermal denaturation studies of triplexes at different pH values[a]

		T_m/°C			
		pH 6.0		pH 6.8	
		T_m1	T_m2	T_m1	T_m2
ON9	5′-TTT TCT TTT CCC CCC T	25.0/22.5[b]	69.0	11.5/<10[c]	69.0
ON10	5′-TTT **X**C**X** TTT CCC CCC T	16.5/15.5[b]	69.0	<10/<10	69.0
ON11	5′-T**X**T **X**C**X** T**X**T CCC CCC T	<10/<10	69.0	<10/<10	69.0
ON12	5′-CTC TTC TTT TCT TTC	43.0/37.5[b,d]	73.0	26.0/<10[c]	72.5
ON13	5′-CTC TTC **X**TT **X**CT TTC	26.0/17.5[b,d]	73.0	<10/<10	72.5
ON14	5′-CTC **X**TC **X**TT **X**CT **X**TC	<10/<10[d]	73.0	<10/<10	72.5

[a] Thermal denaturation temperatures (T_m-values) of **ON9**–**ON11** towards DNA duplex 5′-CCA CTT TTT *AAA AGA AAA GGG GGG A*CT GG:3′-GGT GAA AAA *TTT TCT TTT CCC CCC T*GA CC and of **ON12**–**ON14** towards DNA duplex 5′-GCG C*GA GAA GAA AAG AAA G*CC GG:3′-CGC G*CT CTT CTT TTC TTT C*GG CC measured as the maximum of the first derivative of the melting curve (A_{260} vs temperature) recorded at pH 6.0 [10 mM sodium cacodylate, 150 mM NaCl and 10 mM $MgCl_2$] and pH 6.8 [10 mM sodium cacodylate, 200 mM NaCl and 2 mM $MgCl_2$] using 1.0 μM concentrations of all three strands and a temperature ramp of 0.5 °C/min. T_m values are averages of at least two measurements.

[b] Hysteresis was observed. Left T_m-value observed during heating, right T_m-value observed during cooling.

[c] No hyperchromicity was observed during cooling.

[d] Lowering the temperature ramp to 0.2 °C/min resulted in the following T_m1 values (°C) at pH 6.0: **ON12**: 41.5/37.0; **ON13**: 24.5/20.0; **ON14**: <10/<10. T_m2 values were unaffected.

monophasic transitions similar to the unmodified reference duplexes (see Fig. S1 for a representative example). Incorporation of a single monomer **X** into the mixed sequence 9-mer ONs **ON3**–**ON5** or thymidine-rich 12-mer ONs **ON7**–**ON8** previously used to evaluate LNA, α-L-LNA or ONA monomers,[10,15,38] resulted in dramatically decreased thermal affinities towards DNA complements, compared to unmodified reference ONs (ΔT_m/mod = −17.0 to −14.5 °C). Less pronounced destabilization was observed for duplexes with complementary RNA (ΔT_m/mod = −13.0 to −11.5 °C). Multiple incorporations of monomer **X** into ONs resulted in roughly additive destabilizations of duplexes with DNA/RNA complements.

Thermal denaturation studies were carried out for **ON3** towards DNA and RNA strands with a centrally placed mismatched nucleoside, to investigate if the thymine moiety of monomer **X** base pairs with its complementary nucleotide. Excellent discrimination was observed for T:C and T:T/U mismatches while very poor discrimination of T:G mismatches was observed (Table 1, footnotes c and d).

Comparison of α-L-ONA with LNA, α-L-LNA or ONA (Fig. 1),[10,15,38] clearly demonstrates that α-L-ONA (Fig. 1) has the lowest affinity towards DNA/RNA complements in this series of bicyclic nucleosides. In fact, the mismatch data for α-L-ONA suggest that the thymine moiety of monomer **X** is not base pairing with its counterpart per se but rather recognizes its 'binding' partner merely by size discrimination.

2.4. Triplex thermal denaturation studies

Due to the potential of LNA,[21–24] α-L-LNA[25] and 2′,5′-NAs[35] as TFOs, it was decided to evaluate monomer **X** in this context as well. Thus, **X** monomers were incorporated in 15-mer and 16-mer polypyrimidine sequences (**ON10**–**ON11** and **ON13**–**ON14**, Table 2) previously used to assess the potential of LNA[23], α-L-LNA[25] and ONA[40] as TFOs. Binding to 29-mer and 26-mer double-stranded DNA (for **ON10**–**ON11** and **ON13**–**ON14**, respectively) with internal target sequences in parallel orientation (pyrimidine motif) via Hoogsteen base pairing was evaluated using two different sets of conditions, that is, at pH 6.0 (10 mM sodium cacodylate, 150 mM NaCl and 10 mM $MgCl_2$) and at pH 6.8 (10 mM sodium cacodylate, 200 mM NaCl and 2 mM $MgCl_2$). All ternary complexes exhibit a smooth sigmoidal transition at high temperature corresponding to dissociation of the duplex (T_m2), while no triplex to duplex transition (T_m1) above 10 °C could be observed for **ON10**–**ON11**, **ON13** or **ON14** at pH 6.8.

At pH 6.0, the thermal denaturation curves with reference **ON9** and **ON12** as well as of the doubly modified **ON10** and **ON13** displayed biphasic transitions. Incorporation of two **X** monomers into TFOs resulted in significantly decreased thermal affinities compared to unmodified reference TFOs (ΔT_m/mod = −4.5 to −8.5 °C). Incorporation of four monomers **X** into TFOs accentuated this trend even further as highly destabilized triplexes with T_m1 values below 10 °C were observed. It is noteworthy that all ternary complexes displaying triplex transitions, including the reference strands (also at pH 6.8), exhibited significant thermal hysteresis (see e.g., **ON12**, Table 2), which indicates very slow association kinetics. Even when the temperature ramp was decreased from 0.5 to 0.2 °C/min, hysteresis was observed albeit less pronounced (Table 2, footnote d).

Compared to the properties of LNA and α-L-LNA, the present results indicate that α-L-ONA has a very limited potential as a modification for antisense or antigene strategies.

2.5. Molecular modelling

A series of force field calculations were performed to rationalize the observed trends in thermal affinity of ONs with incorporations of monomer **X**, towards DNA/RNA complements, and furthermore, to place these results in perspective to the reported properties of LNA, α-L-LNA and ONA (Fig. 1) and the suggested inverse relationship between nucleotide geometry (*N*- vs *S*-type) and the nature of phosphodiester linkage (2′,5′- vs 3′,5′-NAs).

Standard B-type DNA:DNA duplexes (5′-GTG A*T*A TGC:3′-CAC TAT ACG) with a single central insertion (italics) of an LNA, α-L-LNA, ONA or **X** monomer, were subjected to molecular dynamics simulation and minimization using the AMBER force field as implemented in MacroModel V9.1.[48] Subsequently, the lowest energy structures of the modified and unmodified duplexes were compared. In the lowest energy structures, LNA and α-L-LNA monomers adopt conformations identical to published NMR solution structures,[19,49] thereby validating the applied modelling protocol. The inverted configurations of the C2′, C3′ and C4′-atoms of α-L-LNA and α-L-ONA, relative to normal DNA, render comparisons based on furanose configurations irrelevant. Instead, a comparison of the obtained structures was made by superimposing the following atoms onto the corresponding unmodified DNA monomer of **ON1**:**ON2** (Fig. 4): (a) the two nucleobase atoms of the modified nucleotide participating in hydrogen bonding (N3 and O4), (b) the C3′-atom of the preceding nucleotide ($C3'_{i-1}$, *i* designating the modified monomer) and (c) the C4′-atom of the subsequent nucleotide ($C4'_{i+1}$).

The central segment of the lowest energy structure of the α-L-ONA modified DNA duplex is significantly perturbed relative to the reference duplex (Fig. 4). Thus, a very extended intrastrand P–P distance (7.8 Å) and a parallel displacement of the nucleobase in radial direction away from the helical axis is observed.

To investigate if the α-L-*ribo* configuration per se leads to the poor accommodation in the helix and to the highly extended nucleotide conformation of α-L-ONA, a comparison was made with the α-L-LNA monomer. However, as previously observed,[15] O5′, O3′ and N1, as well as the C5′-atom and the attached phosphodiester group of α-L-LNA superimpose seamlessly onto the reference DNA strand, despite the inversion of configuration at the C4′-position of α-L-LNA (Fig. 4).

Incorporation of α-L-ONA or α-L-LNA in a β-D-DNA duplex, alters the torsion angle γ (O5′–C5′–C4′–C3′) from +*sc* (~60°), as observed in β-D-*ribo* configured nucleotides,[8] to *ap* (~180°). This has a profound effect on the intrastrand P–P distance, as can be observed with α-L-ONA. In an attempt to further rationalize the effect of changing from β-D-*ribo* to α-L-*ribo* configuration, scrutiny of molecular models indicates that the established

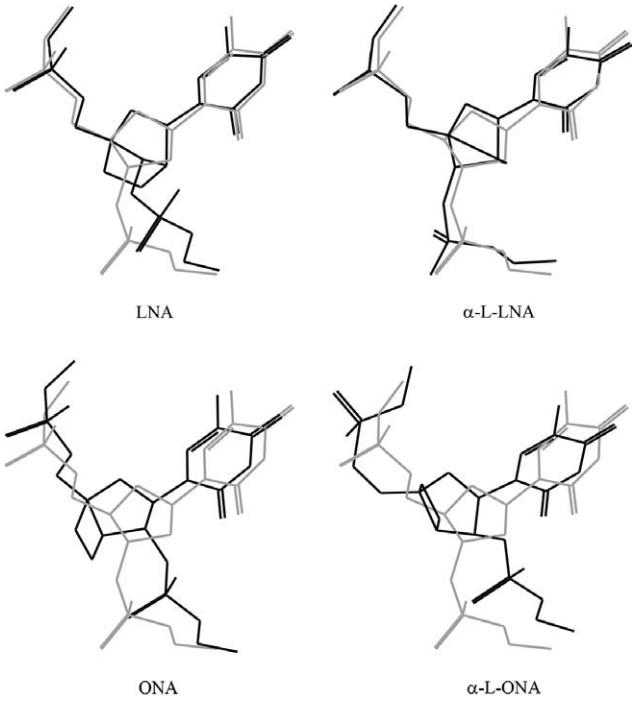

Figure 4. Section of the lowest energy structure (from $C3'_{i-1}$ to $C4'_{i+1}$) obtained from molecular modelling of LNA, α-L-LNA, ONA and α-L-ONA (Monomer **X**) (black line), including overlay of the corresponding DNA structure (The furanose of the unmodified central thymidine in **ON1**:**ON2** is in an *E*-type conformation ($P = 97°$, O4′-*endo*) and not in the expected predominant *S*-type conformation) (grey line).

rules of compact versus extended nucleotide conformations may not be applicable when considering α-L-*ribo* configured nucleotides. 2′,5′-Linked α-L-*ribo* configured nucleotides seem to adopt an extended conformation (P–P distance ~ 7.0 Å) when having a formal *N*-type furanose pucker (overlaying an *S*-type furanose pucker in β-D-*ribo* configured nucleotides). In contrast, they adopt an even further extended conformation (P–P distance >7.5 Å) when having a formal *S*-type furanose pucker. Molecular modelling suggests that the oxetane moiety of monomer X drives the nucleotide towards a more extended conformation ($P = 265°$ and P–P distance ~ 7.8 Å, thus overlaying an *E*-type furanose pucker in β-D-*ribo* configured nucleotides) rather than a more compact conformation as might be anticipated from the established inverse relationship between nucleotide geometry and phosphodiester linkage (Fig. 2). The very extended conformation adopted by α-L-ONA (Fig. 4) necessitates major rearrangements of the backbone, leading to a strained backbone with unfavourable torsion angles, which may explain the observed dramatic decreases in thermal stability of duplexes modified with monomer **X**.

Similarly, the oxetane moiety of ONA disfavours a perfect *S*-type furanose configuration, whereby the conformation is driven away from a conformation mimicking LNA and towards an extended nucleotide conformation ($P = 137°$ and P–P ~ 7.4 Å).

To conclude, α-L-ONA and ONA are not 2′,5′-linked structural mimics of α-L-LNA and LNA, respectively. In addition, intrastrand P–P distances are longer than might have been expected, and these divergences may suggest why ONA and particularly α-L-ONA do not exhibit the same thermal stabilization of modified DNA:DNA duplexes as observed with LNA and α-L-LNA, respectively.

3. Experimental

3.1. General methods

All reagents and solvents were of analytical grade and used without further purification as obtained from commercial suppliers, except for CH_2Cl_2, which was distilled before use. Petroleum ether of the distillation range 60–80 °C was used. Anhydrous DMF and pyridine were used directly as obtained from suppliers. Anhydrous acetonitrile was dried through storage over activated 3 Å molecular sieves. 1,2-Dichloroethane, CH_2Cl_2, *N*,*N*-diisopropylethylamine, dioxane and THF for use in anhydrous reactions were dried through storage over activated 4 Å molecular sieves. Reactions were conducted under an atmosphere of argon whenever anhydrous solvents were used. All reactions were monitored by thin-layer chromatography (TLC) using silica gel coated plates (analytical SiO_2-60, F-254). The TLC plates were visualized under UV light and by dipping in either (a) a 5% concd sulfuric acid in absolute ethanol (v/v) or (b) a solution of molybdato-phosphoric acid and cerium(IV) sulfate (5 g/L) in 3% concd sulfuric acid in water (v/v) followed by heating with a heat gun. Column chromatography using moderate pressure (pressure ball) was performed with Silica Gel 60 (particle size 0.040–0.063 mm, Merck). Evaporation of solvents was carried out under reduced pressure at a temperature below 50 °C. After column chromatography, appropriate fractions were pooled and dried at high vacuum for at least 12 h to give obtained products in high purity (>95%) unless otherwise stated. ^{13}C NMR or ^{31}P NMR ascertained sample purity. ^{1}H NMR, ^{13}C NMR and ^{31}P NMR were recorded at 300, 75.5 and 121.5 MHz, respectively. Chemical shifts are reported in parts per million relative to deuterated solvent as internal standard (δ_H: DMSO-d_6 2.50 ppm; δ_C: DMSO-d_6 39.43 ppm) or external standard (δ_P: 85% H_3PO_4 0.00 ppm). Designation in spectra is as follows: singlet (s), doublet (d), multiplet (m) and broad (br). Exchangeable (ex) protons were detected by disappearance of peaks upon addition of D_2O. Assignments of NMR spectra are based on correlation spectroscopy 2D spectra (H–H correlated (COSY) and H–C correlated (HETCOR)) and follow the standard nucleoside nomenclature. In general, quaternary carbons in ^{13}C NMR spectra were not assigned. The carbon atom of C4 substituents is numbered C5″ in nucleoside derivatives. Similar conventions apply for the corresponding hydrogen atoms. Systematic compound names for bicyclic nucleosides are given according to the von Baeyer nomenclature.[50] MALDI-HRMS were recorded in positive ion mode on a IonSpec FT mass spectrometer using 2,5-dihydroxy benzoic acid as a matrix.

3.2. 1-[5′-*O*-Methanesulfonyl-4′-*C*-methanesulfonyloxymethyl-α-L-*erythro*-pentofuranosyl]thymine (2)

To a solution of alcohol **1**[42] (6.40 g, 11.98 mmol) in EtOAc (120 mL) was added 20% $Pd(OH)_2/C$ (2.01 g). The resulting mixture was evacuated and a H_2 atmosphere was applied, whereafter the mixture was stirred under a H_2 atmosphere for 7 h at rt. The mixture was then filtered through a Celite pad, which was thoroughly washed with EtOAc. The combined organic phase was evaporated to afford diol **2** (4.92 g, 92%) as a white foam. $R_f = 0.2$ (15% *i*-PrOH in CH_2Cl_2, v/v); ^{1}H NMR (DMSO-d_6): δ 11.33 (br s, 1H, ex, NH), 7.57 (d, $J = 1.1$ Hz, 1H, H6), 6.09 (d, $J = 4.0$ Hz, 1H, H1′), 5.80 (d, $J = 4.8$ Hz, 1H, ex, 2′-OH), 5.72 (d, $J = 5.9$ Hz, 1H, ex, 3′-OH), 4.72 (d, $J = 11.0$ Hz, 1H, H5″), 4.42 (dd, $J = 5.9$, 4.7 Hz, 1H, H3′), 4.29–4.35 (m, 3H, H5″/H5′), 4.21 (m, 1H, H2′), 3.26 (s, 3H, CH_3SO_2), 3.24 (s, 3H, CH_3SO_2), 1.76 (d, $J = 1.1$ Hz, 3H, CH_3); ^{13}C NMR (DMSO-d_6): δ 163.7, 150.4, 138.0 (C6), 107.4, 84.5 (C1′), 81.5, 71.8 (C3′), 70.2 (C2′), 69.1 (C5″), 68.6 (C5′), 36.9 (CH_3SO_2), 36.6 (CH_3SO_2), 12.1 (CH_3). Assignment of ^{1}H NMR signals of H5′ and H5″, and of the corresponding ^{13}C NMR signals, may be interchanged. MALDI-HRMS *m*/*z* calcd for $[C_{13}H_{20}N_2O_{11}S_2]Na^+$: 467.0384. Found 467.0401.

3.3. (1*S*,3*R*,4*S*,5*R*)-1-Benzoyloxymethyl-4-hydroxy-3-(thymin-1-yl)-2,6-dioxabicyclo[3.2.0]heptane (3)

A solution of diol **2** (4.54 g, 10.22 mmol) in water (200 mL) was cooled to 0 °C in an ice-bath and aqueous NaOH (2.0 M, 30 mL) was added dropwise. The resulting mixture was stirred at 4 °C for 22 h during which the otherwise clear solution turned brown. The reaction mixture was neutralized by addition of saturated aqueous NH_4Cl, extracted with EtOAc (8×150 mL), and the combined organic phase was evaporated to dryness. The resulting residue was adsorbed on Kieselguhr and purified by silica gel column chromatography (0–15% *i*-PrOH in $CHCl_3$, v/v) affording a mixture of two compounds tentatively assigned as (1*S*,3*R*,4*S*,5*R*)-4-hydroxy-1-methanesulfonyloxymethyl-3-(thymin-1-yl)-2,6-dioxabicyclo[3.2.0]heptane and (1*S*,3*R*,4*S*,7*R*)-7-hydroxy-1-methanesulfonyloxymethyl-3-(thymin-1-yl)-2,5-dioxabicyclo[2.2.1]heptane (2.12 g, ~3:2 ratio by ^{1}H NMR) as a white foam.

The obtained mixture was dissolved in anhydrous DMF (110 mL) and NaOBz (1.68 g, 11.6 mmol) was added. The resulting mixture was stirred at 60 °C for 18 h, whereafter a second portion of NaOBz (400 mg, 2.78 mmol) was added and the temperature raised to 75 °C. After stirring for an additional 19 h, the reaction mixture was cooled to rt and insoluble residues were filtered off and washed extensively with EtOAc. The combined filtrate was evaporated to near dryness and the residue was partitioned between EtOAc (75 mL) and H_2O (50 mL). The phases were separated, and after extraction of the aqueous phase with EtOAc (4×50 mL), the combined organic phase was evaporated to dryness. The resulting residue was adsorbed on Kieselguhr and purified by silica gel column chromatography (0–10% *i*-PrOH in CH_2Cl_2, v/v) to afford alcohol **3** (0.97 g, 25% over two steps) as a white foam. $R_f = 0.4$ (10% *i*-PrOH in CH_2Cl_2, v/v); ^{1}H NMR (DMSO-d_6): δ 11.36 (br s, 1H, ex, NH), 8.09 (d, $J = 0.9$ Hz, 1H, H6), 7.94–8.00 (m, 2H, Ph), 7.65–7.72 (m, 1H, Ph), 7.51–7.59 (m, 2H, Ph), 6.48 (d, $J = 7.0$ Hz, 1H, H1′), 5.87 (br s, 1H, ex, 2′-OH), 5.23 (d, $J = 5.1$ Hz, 1H, H3′), 4.85 (d, $J = 7.9$ Hz, 1H, $H5''_B$), 4.57–4.65 (m, 1H, H2′), 4.45–4.55 (m, 2H, H5′), 4.27 (d, $J = 7.9$ Hz, 1H, $H5''_A$), 1.78 (d, $J = 0.9$ Hz, 3H, CH_3); ^{13}C NMR (DMSO-d_6): δ 165.3, 163.6, 151.4, 139.9 (C6), 133.5 (Ph), 129.2 (Ph), 129.0 (Ph), 128.8 (Ph), 107.9, 86.6 (C1′), 85.6 (C3′), 83.4, 75.8 (C5″), 71.2 (C2′), 64.2 (C5′), 12.3 (CH_3); MALDI-HRMS *m*/*z* calcd for $[C_{18}H_{18}N_2O_7]Na^+$: 397.1006. Found 397.0988.

Physical data for the mixture tentatively assigned as (1*S*,3*R*,4*S*,5*R*)-4-hydroxy-1-methanesulfonyloxymethyl-3-(thymin-1-yl)-2,6-dioxabicyclo[3.2.0]heptane (α-L-ONA derivative) and (1*S*,3*R*,4*S*,7*R*)-7-hydroxy-1-methanesulfonyloxymethyl-3-(thymin-1-yl)-2,5-dioxabicyclo-[2.2.1]heptane (α-L-LNA derivative): Selected signals ^{1}H NMR (DMSO-d_6): δ 6.44 (d, $J = 7.0$ Hz, $H1'_{\alpha\text{-L-ONA}}$), 6.17 (d, $J = 4.0$ Hz, ex, $3'\text{-OH}_{\alpha\text{-L-LNA}}$), 5.95 (s, $H1'_{\alpha\text{-L-LNA}}$), 5.85 (d, $J = 5.1$ Hz, ex, $2'\text{-OH}_{\alpha\text{-L-ONA}}$), 5.12 (d, $J = 5.1$ Hz, $H3'_{\alpha\text{-L-ONA}}$), 4.60–4.38 (m, incl. $H2'_{\alpha\text{-L-ONA}}$, $H3'_{\alpha\text{-L-LNA}}$), 4.27 (s, $H2'_{\alpha\text{-L-LNA}}$); MALDI-HRMS *m*/*z* calcd for $[C_{12}H_{16}N_2O_8S]Na^+$: 371.0520. Found 371.0514.

3.4. (1*R*,3*R*,4*S*,5*R*)-4-Hydroxy-1-hydroxymethyl-3-(thymin-1-yl)-2,6-dioxabicyclo[3.2.0]heptane (4)

Alcohol **3** (0.92 g, 2.47 mmol) was dissolved in satd NH_3/CH_3OH (20 mL) and the resulting mixture was stirred at rt for 28 h, whereupon the solvent was evaporated. Adsorption of the residue on Kieselguhr and purification by silica gel column chromatography (0–10% CH_3OH in CH_2Cl_2, v/v) afforded diol **4** (0.56 g, 84%) as a white solid material. $R_f = 0.3$ (15% CH_3OH in CH_2Cl_2, v/v); ^{1}H NMR (DMSO-d_6): δ 11.31 (br s, 1H, ex, NH), 8.07 (d, $J = 0.9$ Hz, 1H, H6), 6.40 (d, $J = 7.0$ Hz, 1H, H1′), 5.73 (d, $J = 5.1$ Hz, 1H, ex, 2′-OH), 5.05 (t, $J = 5.9$ Hz, 1H, ex, 5′-OH), 5.02 (d, $J = 5.1$ Hz, 1H, H3′), 4.69 (d, $J = 7.7$ Hz, 1H, $H5''_B$), 4.41–4.49 (m, 1H, H2′), 4.12 (d, $J = 7.7$ Hz, 1H, $H5''_A$), 3.42–3.58 (m, 2H, H5′), 1.77 (d, $J = 0.9$ Hz, 3H, CH_3); ^{13}C NMR (DMSO-d_6): δ 163.3, 151.4, 140.0 (C6), 107.6, 86.6, 86.4 (C1′), 85.5 (C3′), 75.5 (C5″), 71.3 (C2′), 60.9 (C5′), 12.3 (CH_3); MALDI-HRMS *m*/*z* calcd for $[C_{11}H_{14}N_2O_6]Na^+$: 293.0744. Found 293.0758.

3.5. (1*S*,3*R*,4*S*,5*R*)-1-(4,4′-Dimethoxytrityloxymethyl)-4-hydroxy-3-(thymin-1-yl)-2,6-dioxabicyclo[3.2.0]heptane (5)

Nucleoside diol **4** (0.38 g, 1.40 mmol) was co-evaporated with anhydrous pyridine (2×10 mL), dissolved in anhydrous pyridine (15 mL) and 4,4′-dimethoxytrityl chloride (0.55 g, 1.61 mmol) was added. The resulting mixture was stirred at rt for 100 min, whereafter a second portion of 4,4′-dimethoxytrityl chloride (160 mg, 0.47 mmol) was added. After stirring at rt for additional 70 min, CH_3OH (2.0 mL) was added and the resulting mixture was evaporated to near dryness. The residue was co-evaporated with toluene/absolute EtOH (10 mL, 1:1 v/v), and EtOAc (30 mL) was added. The organic phase was washed successively with satd aq $NaHCO_3$ (2×20 mL) and brine (15 mL), and the combined aqueous phases were extracted with EtOAc (15 mL). The combined organic phase was evaporated to near dryness, and the residue co-evaporated with toluene/absolute EtOH (10 mL, 50:50, v/v) and absolute EtOH (2×10 mL). The resulting residue was purified by silica gel column chromatography (0–3% CH_3OH in CH_2Cl_2, v/v containing 1 v% pyridine) and co-evaporated with toluene/absolute EtOH (10 mL, 50:50, v/v) and absolute EtOH (2×10 mL) to afford alcohol **5** (0.68 g, 85%) as a white foam. $R_f = 0.3$ (5% CH_3OH in CH_2Cl_2, v/v); ^{1}H NMR (DMSO-d_6): δ 11.37 (br s, 1H, ex, NH), 8.03 (s, 1H, H6), 7.19–7.41 (m, 10H, Ar), 6.86–6.95 (m, 4H, Ar), 6.53 (d, $J = 7.0$ Hz, 1H, H1′), 5.80 (d, $J = 5.5$ Hz, 1H, ex, 2′-OH), 5.01 (d, $J = 5.5$ Hz, 1H, H3′), 4.53–4.62 (m, 2H, H2′, $H5''_B$), 4.16, (d, $J = 7.3$ Hz, 1H, $H5''_A$), 3.74 (s, 6H, CH_3O), 3.22 (s, 2H, H5′), 1.78 (s, 3H, CH_3); ^{13}C NMR (DMSO-d_6): δ 163.6, 158.1, 151.3, 144.5, 139.8 (C6), 135.2, 135.1, 129.6 (Ar), 127.8 (Ar), 127.5 (Ar), 126.7 (Ar), 113.2 (Ar), 107.8, 86.7 (C1′), 85.8, 85.5 (C3′), 84.6, 75.9 (C5″), 71.5 (C2′), 63.3 (C5′), 54.9 (CH_3O), 12.3 (CH_3); MALDI-HRMS *m*/*z* calcd for $[C_{13}H_{20}N_2O_{11}S_2]Na^+$: 595.2051. Found 595.2059.

3.6. (1*S*,3*R*,4*S*,5*R*)-4-[2-Cyanoethoxy(diisopropylamino)-phosphinoxy]-1-(4,4′-dimethoxytrityloxymethyl)-3-(thymin-1-yl)-2,6-dioxabicyclo[3.2.0]heptane (6)

Alcohol **5** (247 mg, 0.43 mmol) was co-evaporated with anhydrous CH_2Cl_2 (2×2 mL), and dissolved in

anhydrous CH_2Cl_2 (2.0 mL). Anhydrous diisopropylethylamine (0.5 mL) and 2-cyanoethyl *N*,*N*-diisopropylphosphoramidochloridite (150 μL, 0.67 mmol) were added. After stirring at rt for 3 h, additional 2-cyanoethyl *N*,*N*-diisopropylphosphoramidochloridite (150 μL, 0.67 mmol) was added. After stirring for a further 28 h, absolute EtOH (2 mL) was added and the resulting mixture was stirred for 25 min. CH_2Cl_2 (20 mL) was added and the organic phase was washed successively with satd aq $NaHCO_3$ (10 mL) and brine (10 mL). The combined aqueous phase was extracted with CH_2Cl_2 (10 mL), and the combined organic phase evaporated to dryness. The resulting residue was purified by silica gel column chromatography (0–40% acetone in petroleum ether, v/v containing 1 v% pyridine) affording **6** (195 mg, 58%) as a white solid material. $R_f = 0.4$ (50% acetone in petroleum ether, v/v); ^{31}P NMR ($CDCl_3$) δ 153.6, 151.5.

3.7. Synthesis of modified oligonucleotides

Synthesis of ONs containing monomer **X** was performed in 0.2 μmol scale using an Applied Biosystems automated DNA synthesizer. Standard procedures were used resulting in stepwise coupling yields >98% of phosphoramidite **6** (20 min coupling time) and >99% of unmodified deoxyribonucleotide phosphoramidites (2 min coupling time) using 1 *H*-tetrazole as catalyst. Removal of nucleobase protecting groups and cleavage from solid support was effected using 32% aq ammonia for 12 h at 55 °C. Detritylation was effected using 80% aq acetic acid for 20 min at rt. Crude ONs were subsequently precipitated from absolute EtOH (−18 °C, 12 h) and washed with 96% EtOH. Composition and purity (>80%) of the synthesized ONs were verified by MALDI-MS analysis and analytical ion-exchange HPLC, respectively.

3.8. Thermal denaturation studies

Concentrations of ONs were calculated using the following extinction coefficients (OD_{260}/μmol): dG, 12.0; dA, 15.2; T, 8.4; dC, 7.1; G, 13.7; A, 15.4; U, 10.0; C, 9.0. Thermal denaturation temperatures (T_m values/°C) were measured on a Perkin–Elmer Lambda 35 UV/VIS spectrometer equipped with a PTP-6 Peltier temperature programmer and determined as the maximum of the first derivative of the thermal denaturation curve (A_{260} vs temperature). Thermal denaturation studies of duplexes were recorded in either medium salt phosphate buffer (100 mM NaCl, 0.1 mM EDTA and pH 7.0 adjusted with 10 mM NaH_2PO_4/5 mM Na_2HPO_4) or high salt phosphate buffer (700 mM NaCl, 0.1 mM EDTA and pH 7.0 adjusted with 10 mM NaH_2PO_4/5 mM Na_2HPO_4). Thermal denaturation studies of triplexes were performed using cacodylate buffer at either pH 6.8 (10 mM sodium cacodylate, 200 mM NaCl, 2 mM $MgCl_2$, and pH 6.8 adjusted by addition of dilute aq HCl) or cacodylate buffer at pH 6.0 (10 mM sodium cacodylate, 150 mM NaCl, 10 mM $MgCl_2$ and pH 6.0 adjusted by addition of dilute aq HCl). For studies of duplexes as well as triplexes, ONs (1.0 μM each strand) were thoroughly mixed, denatured by heating to 90 °C and subsequently cooled to the starting temperature of the experiment. The absorbance was measured at 0.5 °C intervals using 1 mL quartz optical cells with a path length of 1.0 cm. The temperature of the denaturation experiments ranged from at least 15 °C below T_m to 15 °C above T_m (although not below 5 °C or above 85 °C). A temperature ramp of 1.0 °C/min was used in all experiments studying duplex transitions, whereas a temperature ramp of 0.5 or 0.2 °C/min was for triplex studies. Reported thermal denaturation temperatures are an average of at least two measurements within ±1.0 °C.

3.9. Molecular modelling

Duplex **ON1**:**ON2** was built with a standard B-type helical geometry using the Amber software suite and subsequently modified to the duplexes of interest within the MacroModel V9.1 Suite of programs.[48] The charge of the phosphodiester backbone was neutralized with sodium ions, which were placed 3.0 Å from the negatively charged oxygen atoms in the plane described by the phosphorus and the non-bridging oxygen atoms. During the following molecular dynamics simulation and minimization, the sodium–oxygen distances were restrained to 3.0 Å by a force constant of 418 kJ/molÅ^2. Employing these partial constrictions, the duplex structures were minimized using the Polak–Ribiere conjugate gradient method, the all-atom AMBER force field[51,52] and GB/SA solvation model[53] as implemented in MacroModel V9.1. Non-bonded interactions were treated with extended cut-offs (van der Waals 8.0 Å and electrostatics 20.0 Å). The minimized structures were then (using the same constraints as described above) submitted to 5 ns of stochastic dynamics (simulation temperature 300 K, time step 2.2 fs, SHAKE all bonds to hydrogen), during which 500 structures were sampled and subsequently minimized.

Acknowledgements

We greatly appreciate funding from The Danish National Research Foundation, Villum Kann Rasmussen Fonden and The Oticon Foundation.

Supplementary data

Copies of ^{13}C NMR spectra of nucleotides **1**–**5**, ^{31}P NMR spectrum of phosphoramidite **6**, MALDIMS data

of synthesized ONs (Table S1), representative denaturation curves of **ON3** with complementary DNA/RNA (Fig. S1) and of **ON13** as TFO illustrating the observed thermal hysteresis (Fig. S2). Supplementary data associated with this article can be found, in the online version, at doi:10.1016/j.carres.2006.04.010.

References

1. Opalinska, J. B.; Gewirtz, A. M. *Nat. Rev. Drug Disc.* **2002**, *1*, 503–514.
2. Buchini, S.; Leumann, C. J. *Curr. Opin. Chem. Biol.* **2003**, *7*, 717–726.
3. Kurreck, J. *Eur. J. Biochem.* **2003**, *270*, 1628–1644.
4. Kværnø, L.; Wengel, J. *Chem. Commun.* **2001**, 1419–1424.
5. Leumann, C. J. *Bioorg. Med. Chem.* **2002**, *10*, 841–854.
6. Meldgaard, M.; Wengel, J. *J. Chem. Soc., Perkin Trans. 1* **2000**, 3539–3554.
7. For a recent example, see: Pradeepkumar, P. I.; Cheruku, P.; Plashkevych, O.; Acharya, P.; Gohil, S.; Chattopadhyaya, J. *J. Am. Chem. Soc.* **2004**, *126*, 11484–11499.
8. Saenger, W. *Principles of Nucleic Acid Structure*; Springer: Berlin, 1984.
9. Singh, S. K.; Nielsen, P.; Koshkin, A. A.; Wengel, J. *Chem. Commun.* **1998**, 455–456.
10. Koshkin, A. A.; Singh, S. K.; Nielsen, P.; Rajwanshi, V. K.; Kumar, R.; Meldgaard, M.; Olsen, C. E.; Wengel, J. *Tetrahedron* **1998**, *54*, 3607–3630.
11. Obika, S.; Nanbu, D.; Hari, Y.; Andoh, J.; Morio, K.; Doi, T.; Imanishi, T. *Tetrahedron Lett.* **1998**, *39*, 5401–5404.
12. Wengel, J. *Acc. Chem. Res.* **1999**, *32*, 301–310.
13. Petersen, M.; Wengel, J. *Trends Biotechnol.* **2003**, *21*, 74–81.
14. Rajwanshi, V. K.; Håkansson, A. E.; Dahl, B. M.; Wengel, J. *Chem. Commun.* **1999**, 1395–1396.
15. Rajwanshi, V. K.; Håkansson, A. E.; Sørensen, M. D.; Pitsch, S.; Singh, S. K.; Kumar, R.; Nielsen, P.; Wengel, J. *Angew. Chem., Int. Ed.* **2000**, *39*, 1656–1659.
16. Sørensen, M. D.; Kværnø, L.; Bryld, T.; Håkansson, A. E.; Verbeure, B.; Gaubert, G.; Herdewijn, P.; Wengel, J. *J. Am. Chem. Soc.* **2002**, *124*, 2164–2176.
17. Nielsen, K. E.; Singh, S. K.; Wengel, J.; Jacobsen, J. P. *Bioconjug. Chem.* **2000**, *11*, 228–238.
18. Petersen, M.; Bondensgaard, K.; Wengel, J.; Jacobsen, J. P. *J. Am. Chem. Soc.* **2002**, *124*, 5974–5982.
19. Nielsen, K. M. E.; Petersen, M.; Håkansson, A. E.; Wengel, J.; Jacobsen, J. P. *Chem. Eur. J.* **2002**, *8*, 3001–3009.
20. Nielsen, J. T.; Stein, P.; Petersen, M. *Nucleic Acids Res.* **2003**, *31*, 5858–5867.
21. Obika, S.; Hari, Y.; Sugimoto, T.; Sekiguchi, M.; Imanishi, T. *Tetrahedron Lett.* **2000**, *41*, 8923–8927.
22. Obika, S.; Uneda, T.; Sugimoto, T.; Nanbu, D.; Minami, T.; Doi, T.; Imanishi, T. *Bioorg. Med. Chem.* **2001**, *9*, 1001–1011.
23. Torigoe, H.; Hari, Y.; Sekiguchi, M.; Obika, S.; Imanishi, T. *J. Biol. Chem.* **2001**, *276*, 2354–2360.
24. Sun, B.-W.; Babu, B. R.; Sørensen, M. D.; Zakrzewska, K.; Wengel, J.; Sun, J.-S. *Biochemistry* **2004**, *43*, 4160–4169.
25. Kumar, N.; Nielsen, K. E.; Maiti, S.; Petersen, M. *J. Am. Chem. Soc.* **2006**, *128*, 14–15.
26. Kierzek, R.; He, L.; Turner, D. H. *Nucleic Acids Res.* **1992**, *20*, 1685–1690.
27. Dougherty, J. P.; Rizzo, C. J.; Breslow, R. *J. Am. Chem. Soc.* **1992**, *114*, 6254–6255.
28. Hashimoto, H.; Switzer, C. J. *J. Am. Chem. Soc.* **1992**, *114*, 6255–6256.
29. Giannaris, P. A.; Damha, M. J. *Nucleic Acids Res.* **1993**, *21*, 4742–4749.
30. Alul, R.; Hoke, G. *Antisense Res. Dev.* **1995**, *5*, 3–11.
31. Sheppard, T. L.; Breslow, R. C. *J. Am. Chem. Soc.* **1996**, *118*, 9810–9811.
32. Kandimalla, E. R.; Manning, A.; Zhao, Q.; Shaw, D. R.; Byrn, R. A.; Sasisekharan, V.; Agrawal, S. *Nucleic Acids Res.* **1997**, *25*, 370–378.
33. Wasner, M.; Arion, D.; Borkow, G.; Noronha, A.; Uddin, A. H.; Parniak, M. A.; Damha, M. J. *Biochemistry* **1998**, *37*, 7478–7486.
34. Damha, M. J.; Noronha, A. *Nucleic Acids Res.* **1998**, *26*, 5152–5156.
35. Obika, S.; Hiroto, A.; Nakagawa, O.; Imanishi, T. *Chem. Commun.* **2005**, 2793–2795.
36. Lalitha, V.; Yathindra, N. *Curr. Sci.* **1995**, *68*, 68–75.
37. Premraj, B. J.; Yathindra, N. *J. Biomol. Struc. Dyn.* **1998**, *16*, 313–328.
38. Obika, S.; Morio, K.; Hari, Y.; Imanishi, T. *Bioorg. Med. Chem. Lett.* **1999**, *9*, 515–518.
39. Obika, S.; Morio, K.; Nanbu, D.; Hari, Y.; Itoh, H.; Imanishi, T. *Tetrahedron* **2002**, *58*, 3039–3049.
40. Savy, P.; Benhida, R.; Fourrey, J.-L.; Maurisse, R.; Sun, J.-S. *Bioorg. Med. Chem. Lett.* **2000**, *10*, 2287–2289.
41. Hrdlicka, P. J.; Kumar, T. S.; Wengel, J. *Eur. J. Org. Chem.* **2005**, 5184–5188.
42. Babu, B. R.; Raunak; Poopeiko, N. E.; Juhl, M.; Bond, A. D.; Parmar, V. S.; Wengel, J. *Eur. J. Org. Chem.* **2005**, 2297–2321.
43. Greene, T. W.; Wuts, P. G. M. *Protective Groups in Organic Synthesis*, 3rd ed.; Wiley: New York, 1999, pp 49–54, and references cited therein.
44. Kocienski, P. J. *Protecting Groups*, 3rd ed.; Georg Thieme: Stuttgart, 2005, pp 315–320, and references cited therein.
45. Barma, D. K.; Bandyopadhyay, A.; Capdevila, J. H.; Falck, J. R. *Org. Lett.* **2003**, *5*, 4755–4757.
46. Obika, S.; Morio, K.; Hari, Y.; Imanishi, T. *Chem. Commun.* **1999**, 2423–2424.
47. Hrdlicka, P. J.; Andersen, N. K.; Jepsen, J. S.; Hansen, F. G.; Haselmann, K. F.; Nielsen, C.; Wengel, J. *Bioorg. Med. Chem.* **2005**, *13*, 2597–2621.
48. MacroModel, version 9.1, Schrödinger, LLC, New York, NY, 2005.
49. Nielsen, C. B.; Singh, S. K.; Wengel, J.; Jacobsen, J. P. *J. Biomol. Struct. Dyn.* **1999**, *17*, 175–191.
50. Moss, G. P. *Pure Appl. Chem.* **1999**, *71*, 513–529.
51. Weiner, S. J.; Kollman, P. A.; Case, D. A.; Singh, U. C.; Ghio, C.; Alagona, G.; Profeta, S.; Weiner, P. *J. Am. Chem. Soc.* **1984**, *106*, 765–784.
52. Weiner, S. J.; Kollman, P. A.; Nguyen, D. T.; Case, D. A. *J. Comput. Chem.* **1986**, *7*, 230–252.
53. Still, W. C.; Tempczyk, A.; Hawley, R. C.; Hendrickson, T. *J. Am. Chem. Soc.* **1990**, *112*, 6127–6129.